# Endosomal Size and Membrane Leakiness Influence Proton Sponge-Based Rupture of Endosomal Vesicles

*Lotte M.P. Vermeulen[1,2], Toon Brans[1,2], Sangram K. Samal[1,2], Peter Dubruel[3], Jo Demeester[1], Stefaan C. De Smedt[1], Katrien Remaut[1], Kevin Braeckmans[1,2,*]*

*Address correspondence to Kevin.Braeckmans@UGent.be

[1]Lab. General Biochemistry & Physical Pharmacy, Ghent University, Ghent, Belgium

[2]Centre for Nano- and Biophotonics, Ghent University, Ghent, Belgium

[3]Polymer Chemistry & Biomaterials Group, Ghent University, Ghent, Belgium

**ABSTRACT**

In gene therapy, endosomal escape represents a major bottleneck since nanoparticles often remain entrapped inside endosomes and are trafficked towards the lysosomes for degradation. A detailed understanding of the endosomal barrier would be beneficial for developing rational strategies to improve transfection and endosomal escape. By visualizing individual endosomal escape events in live cells we obtain insight into mechanistic factors that influence proton sponge-based endosomal escape. In a comparative study, we found that HeLa cells treated with JetPEI/pDNA polyplexes have a 3.5-fold increased endosomal escape frequency compared to ARPE-19 cells. We found that endosomal size has a major impact on the escape capacity. The smaller HeLa endosomes are more easily ruptured by the proton sponge effect than the larger ARPE-19 endosomes, a finding supported by a mathematical model based on the underlying physical principles. Still, it remains intriguing that even in the small HeLa endosomes, less than 10% of the polyplex-containing endosomes show endosomal escape. Further experiments revealed that the membrane of polyplex-containing endosomes becomes leaky to small compounds, preventing effective build-up of osmotic pressure, which in turn prevents endosomal rupture. Analysis of H1299 and A549 cells revealed that endosomal size determines endosomal escape efficiency when cells have comparable membrane leakiness. However, at high levels of membrane leakiness build-up of osmotic pressure is no longer possible, regardless of endosomal size. Based on our findings that both endosomal size and membrane leakiness have a high impact on proton sponge-based endosomal rupture, we provide important clues towards further improvement of this escape strategy.

**KEYWORDS: gene therapy · nanomedicine · polyethylenimine · endosomal escape · proton sponge effect**

In recent years, there has been an increasing interest in the cytosolic delivery of macromolecular drugs which in many cases need to be delivered to intracellular (IC) targets to exert their intended function.[1] It is believed that targeted delivery to IC compartments (*e.g.* cytosol, lysosomes, mitochondria, nucleus, …) holds great potential for precision therapeutics,[2] decreasing toxicity while maximizing therapeutic efficiency.[1,3] In order to gain access to the IC environment, therapeutic macromolecules are often incorporated into nanocarriers composed of lipids, polymers or a combination of both. Such nanomedicines are usually internalized by cells through active endocytosis.[4,5] As endocytosis is a natural process for transportation between and within cells, and can be utilized by cells to internalize nutrients or regulate signaling cascades, it poses an ideal pathway for the uptake of compounds that cannot permeate through the cell membrane.[6–8] In the process of endocytosis, the cargo is engulfed in membrane invaginations, leading to the formation of vesicles, called endosomes. Afterwards, the cargo is delivered to specialized vesicular structures to enable sorting and delivery of the cargo to different IC destinations.[5] Upon maturation, endosomes acidify and eventually fuse with lysosomes, leading to degradation of the macromolecular therapeutic cargo by lysosomal digestive enzymes.[1,3,4] To avoid this enzymatic degradation and in order to reach the intended subcellular target site, nanomedicines need to induce escape of their cargo from the endosomes into the cytoplasm.[9] Unfortunately, even when endowed with specially tailored escape mechanisms, only a small fraction of nanoparticles seems capable of crossing the endosomal barrier and endosomal escape remains a crucial rate-limiting step for IC delivery of macromolecules.[2,4,10–12]

Several cationic polymers with an intrinsic endosomolytic activity are believed to escape the endosome *via* the so-called 'proton sponge effect', which is based on the pH buffer capacity of the polymer.[13,14] During endosomal maturation, protons are actively translocated into endosomes by membrane-bound ATPase pumps, which will protonate the polymer, thereby buffering the endosomal lumen. Transfer of protons across the endosomal membrane is accompanied by passive chloride influx to balance charges. The

increasing ionic concentration is accompanied by water influx, which leads to osmotic swelling of the endosome. In this way, the proton sponge effect is believed to finally lead to rupture of the endosomal membrane and release of the endosomal content into the cytoplasm.[15] Recent findings indicate that next to osmotic swelling also membrane destabilization contributes to endosomal membrane rupture.[4,16] Yet, while the proton sponge mechanism has become a central paradigm for polymer-based carriers, it has recently been shown that only a very limited number (as few as 1 up to 5) of internalized polyplexes effectively escape from the endosomes.[16] It would be beneficial to understand why these numbers are limited, since enhancing the endosomal escape capacity of the polyplexes could lower the dose that needs to be administered to obtain a certain transfection level, hence decreasing cytotoxicity that is often related to the use of cationic polymers.[17]

As a means to get further insight into the factors that contribute to effective endosomal escape, we have performed a detailed comparative study of the endosomal escape of JetPEI/pDNA polyplexes in two different cell lines, HeLa cells and ARPE-19 cells. In this fundamental study we made use of polyethylenimine (PEI) since it is the gold standard for proton sponge-based delivery of nucleic acids. While ARPE-19 cells internalize more polyplexes than HeLa cells, the level of transfection in HeLa cells is – surprisingly – much higher. We start by showing that this is linked to a higher frequency of endosomal escape events in HeLa cells as compared to ARPE-19 cells. Therefore, this marked difference between both cell types forms an interesting starting point for exploring intrinsic endosomal properties that affect endosomal escape efficiency. We study endosomal mobility, pH, size and membrane leakiness, leading to the conclusion that both endosomal size and membrane leakiness are very important factors that modulate effective endosomal escape. This finding is further tested on A549 and H1299 cells, which show low endosomal escape frequency due to large endosomal size and endosomal leakiness, respectively. Together our work provides fundamental insights that are crucial to ameliorate proton sponge-based endosomal release and thus transfection efficiency of gene polyplexes.

## RESULTS

### Characterization of polyplexes

JetPEI/pDNA polyplexes were prepared from JetPEI and a mixture of pDNA and AlexaFluor 647 (AF647)-labeled oligonucleotides (ONs) at different N/P ratios (=charge ratio defined as Nitrogen/Phosphate ratio). Gel electrophoresis was performed to evaluate if pDNA and ONs are retained in the polyplexes. As can be seen in **Figure S1A**, starting from N/P 4 both pDNA and ONs are efficiently complexed inside the polyplexes. Next, hydrodynamic diameter, polydispersity index (PdI) and zeta potential of particles with N/P 2, 4, 6 and 8 were measured with dynamic light scattering (**Fig. S1B-C**). JetPEI N/P 6 particles with a size of 108.7 ± 2.6 nm (mean ± SEM) and zeta potential of 31.6 ± 0.3 mV (mean ± SEM) were selected for further experiments.

The purpose of co-incorporating fluorescently labelled ONs into the JetPEI/pDNA complexes is to visualize and quantify endosomal escape according to a recently published dequenching assay.[16,18] When the polyplexes reside in the endosome, the fluorescence of these ONs is effectively quenched. Upon endosomal bursting, the labeled ONs escape from the endosome to the cytoplasm which can be seen as an intense burst of fluorescence, thus allowing to evaluate the number of endosomal escape events in time and space (**Fig. 1A**). A few minutes after endosomal escape, the ON fluorescence spreads towards the entire cytoplasm and eventually accumulates into the nucleus (**Fig. 1B**). The burst and subsequent accumulation in the nucleus provides a double confirmation that endosomal escape has happened. A live-cell movie recorded with a swept field microscope is provided (**Movie S1**; time indicated in hh:mm:ss) to illustrate this assay.

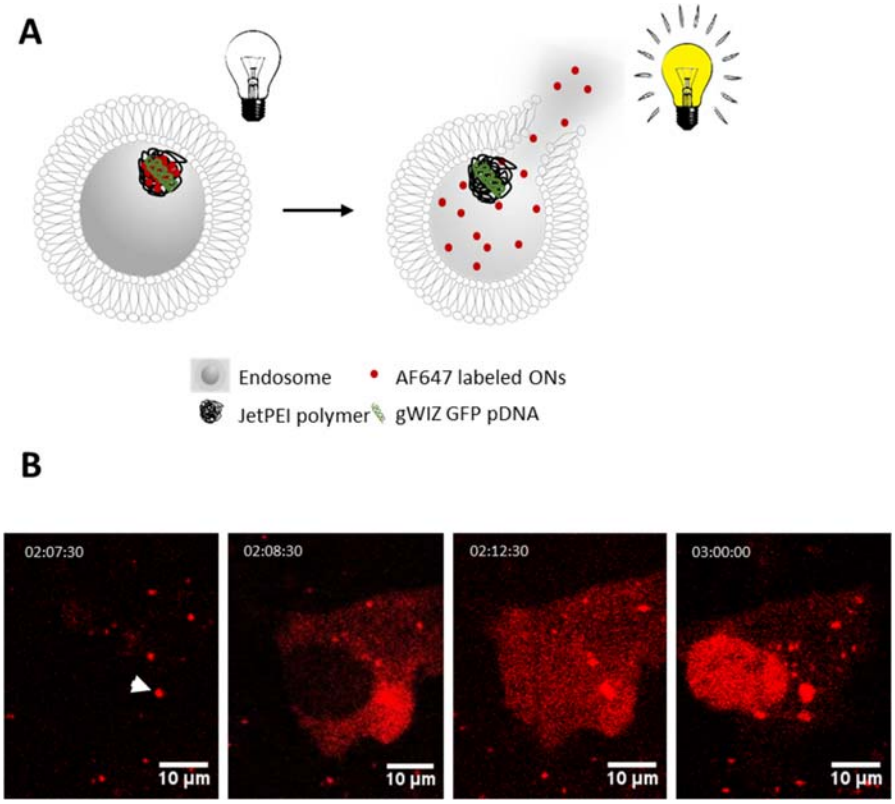


**Fig 1. Dequenching assay to evaluate endosomal escape efficiency of nanoparticles. (A)** Schematic representation of the dequenching assay where the release of AF647 ONs visualizes the time point and place of endosomal bursts. **(B)** Microscopic images of an endosomal escape event. The arrow in the first frame indicates an endosome that contains quenched ONs. In the second frame this endosome has burst, as can be seen from a sudden increase in fluorescence intensity. In the third frame the released ONs spread into the cytoplasm and eventually accumulate into the nucleus (frame 4). Time is indicated in the left upper corner in hh:mm:ss after addition of the JetPEI/pDNA polyplexes.

## Evaluation of transfection efficiency of JetPEI polyplexes in HeLa and ARPE-19 cells

HeLa and ARPE-19 cells were transfected with JetPEI/pDNA N/P 6 polyplexes. The transfection efficiency based on GFP expression was quantified after 24h *via* flow cytometry, showing a marked difference between both cell types. As apparent from both the percentage of GFP positive cells (**Fig. 2A**) as well as the median GFP fluorescence per transfected cell (**Fig. 2B**), HeLa cells were clearly much easier to transfect than ARPE-19 cells when exposed to the same concentration of JetPEI/pDNA polyplexes. This was irrespective of when polyplexes were applied in concentrations equal to 0.67 or 1.00 µg pDNA per 50 000 cells. The difference in transfection efficiency is most obvious from **Figure 2C**, which displays the average GFP content per cell over the entire population (*i.e.* including non-transfected cells). After 48h post

transfection (the cell division time of ARPE-19 cells is 48h[19] *versus* 22h for HeLa cells[20]), the difference in transfection between HeLa cells and ARPE-19 cells was even more pronounced (**Fig. S2**).

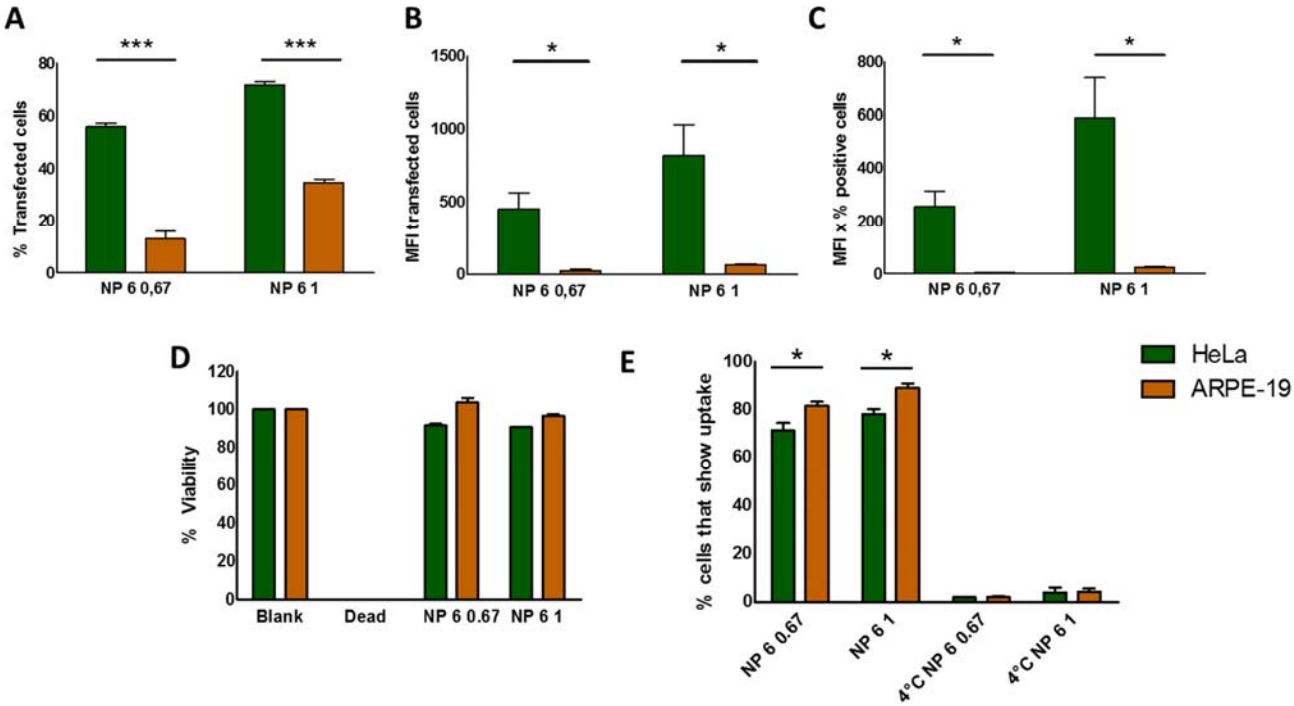


**Fig 2. Measuring transfection efficiency, cell viability and cellular uptake of JetPEI/pDNA polyplexes. (A)** Shows the percentage of cells that are positive for GFP transfection, while **(B)** displays the median GFP fluorescence intensity (MFI) of transfected cells. **(C)** MFI x the percentage of positive cells was calculated to display the average GFP content per cell over the entire population (including untransfected cells). **(D)** Cell viability was measured by means of an MTT test. **(E)** Polyplex uptake was quantified as percentage of positive cells. 4°C controls were included to show that membrane-attached polyplexes do not contribute to the measured signal thanks to Trypan Blue quenching. All graphs show mean ± SEM; n=3. Significance was calculated using student t-tests (transfection, uptake) or one-way ANOVA with Dunnett's post-test (compare means to the value of 80% cell viability) (*** $p < 0.0001$; ** $p < 0.01$; * $p < 0.05$).

This much higher transfection efficiency in HeLa cells could not be explained by a difference in cytotoxicity, as MTT assay showed >80% viability for both cell types (**Fig. 2D**). Second, uptake experiments were carried out to see if a difference in polyplex uptake efficiency may be the cause. Uptake of JetPEI polyplexes was quantified *via* flow cytometry (**Fig. 2E**) and showed a significant increase in polyplex content in ARPE-19 cells *vs* HeLa cells. Since HeLa cells internalize less polyplexes, a difference in uptake clearly cannot account for the higher transfection efficiency.

**The role of endosomal escape**

In further pursuit of an explanation concerning the observed difference in transfection efficiency in HeLa *vs* ARPE-19 cells, we next investigated endosomal escape, which was visualized and quantified by time-lapse confocal microscopy as mentioned above. After a 15 min incubation with JetPEI/pDNA polyplexes, cells were imaged every 30 s for a total time of 6 h. Individual endosomal escape events were observed as sudden intense, localized bursts of light followed by translocation of the labelled ONs to the nucleus (see **Movie S2** (HeLa) and **Movie S3** (ARPE-19) both have time indication in hh:mm:ss). Therefore, the number of cells in which endosomal escape happened at least once could be quantified by counting the number of red fluorescent nuclei. Microscopy images at time point 3 h can be seen in **Figure 3A** and illustrate that endosomal escape occurred in a much greater amount of HeLa than ARPE-19 cells. By analyzing a total of 1308 HeLa and 1052 ARPE-19 cells over time, it was shown that endosomal escape happened in 3.42 ± 0.40 times more HeLa cells as compared to ARPE-19 cells (**Fig. 3B**). Furthermore, it became apparent that endosomal escape predominantly occurred within the first three hours after addition of the polyplexes in both cell types. This marked difference points to the fact that endosomal escape efficiency plays an important role in the difference in transfection efficiency observed for both cell types.

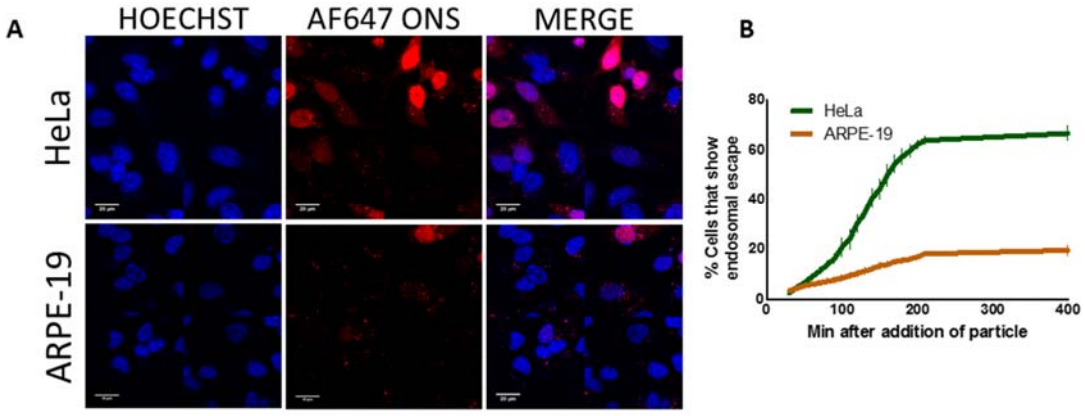


**Fig 3. Evaluating the role of endosomal escape. (A)** Representative confocal images as seen in the dequenching endosomal escape assay 3h after incubation with polyplexes. Hoechst nuclei can be seen in blue, while cells in which endosomal escape occurred show nuclear fluorescence in the red channel due to the release of AF647 ONs from the polyplexes. Scalebar represents 20 µm. **(B)** The number of cells with red nuclei in which endosomal escape has happened at least once are quantified in function of time. Values represent mean ± SEM and statistical analysis was carried out using a student t-test on a total of 1308 HeLa cells and 1052 ARPE-19 cells.

**Exploring the influence of endosomal properties on endosomal escape**

Considering the fact that HeLa cells actually internalized less polyplexes, the question arose as to why endosomal escape was that much more efficient in HeLa cells than in ARPE-19 cells. An answer to this question was sought by investigating the influence of several mechanistic endosomal properties on proton sponge-based endosomal escape.

***Influence of endosomal sequestration, pH and mobility***

First, we investigated if perhaps polyplexes are sequestered at higher concentrations in HeLa endosomes, *e.g.* due to differences in cellular uptake and trafficking pathways. This could be of considerable importance since one could argue that a higher amount of polyplexes within an endosome increases the buffering capacity, making endosomal swelling and bursting more likely to happen. To answer this question we compared the number of polyplex-containing endosomes in both cell types *via* confocal microscopy. It turned out that HeLa cells had 2.11 ± 0.24 times more polyplex-containing endosomes per cell than ARPE-19 cells (**Fig. 4A**). Combined with the fact that HeLa cells internalized a smaller total amount of polyplexes than ARPE-19 cells (**Fig. 2E**), this means that the average number of polyplexes per endosome in HeLa cells is about 3 times less, as schematically presented in **Fig. 4B**. This points to the fact that the higher endosomal escape efficiency in HeLa cells did not simply arise from a higher polyplex load per endosome.

One could argue though that, since HeLa cells have about two times more polyplex-containing endosomes, endosomal escape is twice as likely to happen. To investigate this, we turned back to the endosomal escape movies and determined the number of individual endosomal escape events per cell. Multiple endosomal escape events can indeed happen within the same cell, as shown in **Figure 4C** (arrows indicate places where individual escape events can be seen) and **Movie S4** (time indicated in hh:mm:ss). By image analysis an average of 2.26 ± 0.14 burst events was found per HeLa cell, while for ARPE-19 cells this was only 0.253 ± 0.029 (**Fig. 4D**). Taking into account that HeLa cells have 2 times more polyplex-containing endosomes

per cell, it still means that endosomes in HeLa cells are intrinsically 4.22 ± 0.73 times more likely to burst as compared to ARPE-19 cells (**Figure 4E**). Clearly, other fundamental endosomal properties must play a role, warranting further investigation.

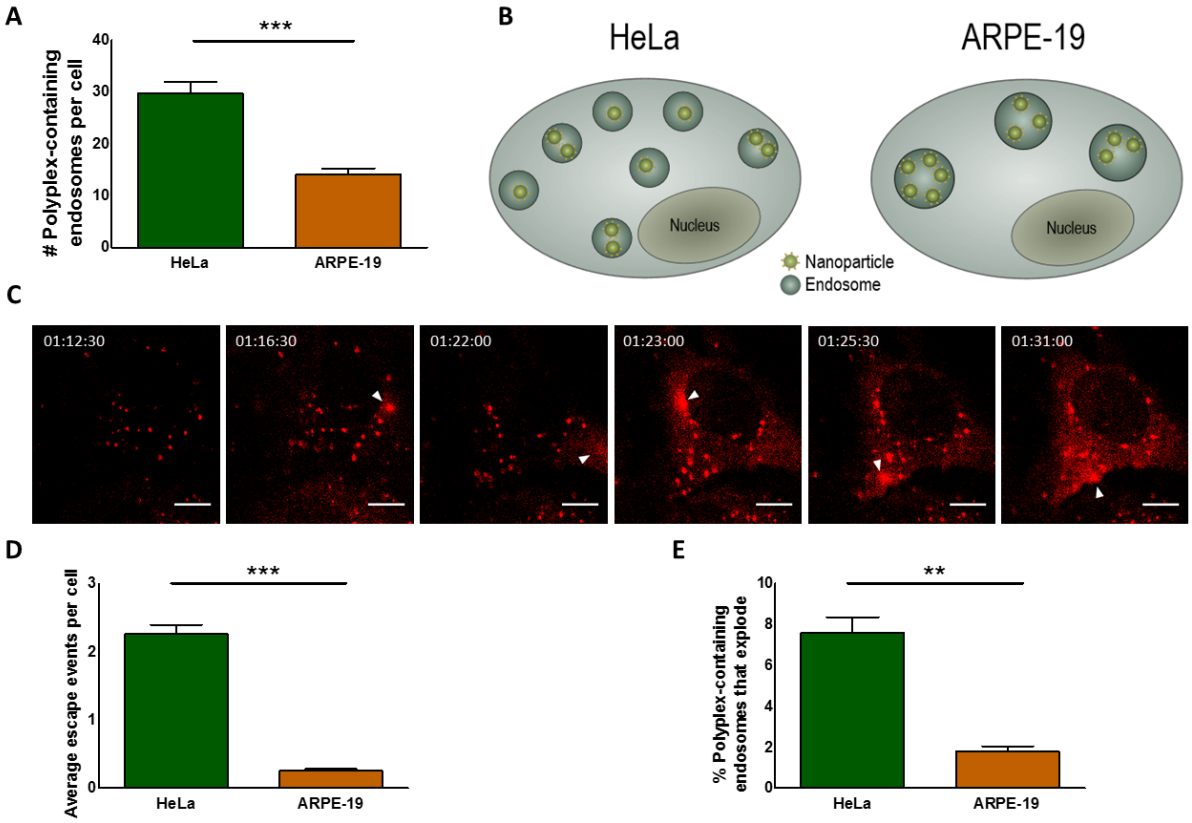


**Fig. 4. Evaluation of the influence of polyplex content per endosome and total number of polyplex-containing endosomes on endosomal escape efficiency in HeLa *vs* ARPE-19 cells. (A)** The graph displays the number of polyplex-containing endosomes per cell that are visible 2 µm above the cover slip in HeLa cells and ARPE-19 cells. Bars represent mean ± SEM based on evaluation of 33 HeLa and 39 ARPE-19 cells. **(B)** Schematic presentation of the distribution of nanoparticles inside endosomes in HeLa *vs* ARPE-19 cells, indicating that the polyplex content per endosomes is lower in HeLa cells than in ARPE-19 cells. **(C)** Confocal images that demonstrate multiple endosomal escape events (white arrows) within one cell over time. Scale bar represents 10 µm. **(D)** The average number of endosomal burst events per cell in a HeLa population *vs* ARPE-19 population is presented. Bars represent mean ± SEM. **(E)** The graph displays the percentage of polyplex-containing endosomes that explode in HeLa cells *vs* ARPE-19 cells. Bars represent mean ± SEM and are calculated using values displayed in Fig. 4A and Fig. 4D. Statistical analysis on all data was performed using student t-tests (*** $p < 0.0001$; ** $p < 0.01$; * $p < 0.05$).

A decrease in pH is the driving factor of endosomal swelling in the proton sponge mechanism. As such it may be that endosomal acidification may be less pronounced in ARPE-19 cells which would lead to less

endosomal swelling and bursting. Results in **Figure 5A** show that ARPE-19 endosomes are actually slightly more acidic than HeLa endosomes, which shows that a difference in pH cannot explain the observed results. Another hypothesis could be that HeLa cells have higher endosomal mobility, which could result in increased shear stress, thus making bursting of swollen endosomes more likely. The instantaneous endosomal velocity (nm/s) of the endosomes was determined by Single Particle Tracking microscopy and is displayed in **Figure 5B** and **Movie S5** (time indicated in mm:ss:ms). Based on these results, no obvious difference between the mobility of endosomes from HeLa cells and endosomes from ARPE-19 cells was observed.

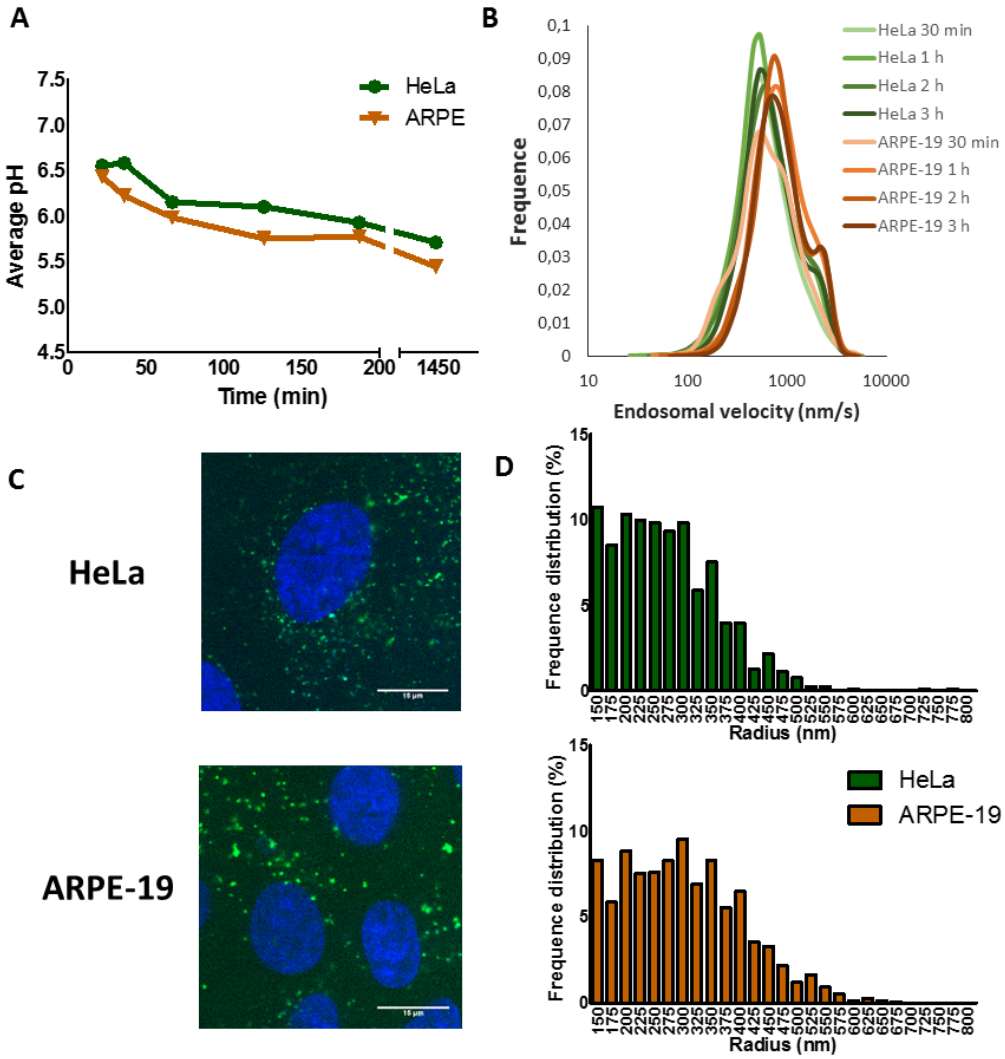

**Fig. 5. Investigating the difference in pH, mobility and size between HeLa and ARPE-19 endosomes to evaluate their influence on the endosomal escape capacity exerted by JetPEI/pDNA polyplexes in these cell types. (A)** The average pH ± SEM at several time points – as measured by confocal microscopy – is displayed for HeLa and ARPE-19 endosomes. Graph is based on the evaluation of 19667 HeLa endosomes and 14862 ARPE-19 endosomes. **(B)** Endosomal velocity – measured by single particle tracking – is depicted. Green lines represent distributions measured in HeLa cells, while orange distributions are measured in ARPE-19 cells. Graph is based on the evaluation of 14980 HeLa endosomes and 12383 ARPE-19 endosomes. **(C)** A representative confocal image of HeLa and ARPE-19 cells is shown to demonstrate the visual difference in endosomal size. Scale bar represents 15 µm. **(D)** The size of 783 HeLa *vs* 1466 ARPE-19 endosomes was measured after incubation with FITC dextrans and subsequent chase with cell culture medium for 3h. Frequency distributions of endosomal radii show a shift to higher endosomal radii, indicating that ARPE-19 cells have more larger endosomes, as is also visually evident from **(C)**.

### *Influence of endosomal size*

Next, we turned our attention to the potential role of endosomal size. Even though endosomes are close to the resolution limit of confocal microscopy, it could be noted that endosomes in ARPE-19 cells appeared bigger than those in HeLa cells. This can be readily appreciated in the confocal images of **Figure 5C**, where endosomes were labeled by fluid phase uptake of 10 kDa FITC-dextran. By image processing, we determined the apparent endosomal size after initial incubation with 10 kDa FITC-dextran and subsequent chase with cell culture medium for 3 h. The endosomal size distribution of 783 HeLa and 1466 ARPE-19 endosomes is shown in **Figure 5D**. Although these radii should not be considered to be absolutely correct given the optical resolution limit, still one can appreciate a relative shift to larger sizes of the ARPE-19 endosomes.

*Understanding the influence of endosomal size on bursting of the endosome: a mathematical model*

To examine the impact of endosomal size on endosomal escape efficiency *via* the proton sponge effect, a simple mathematical model is set up that describes the relation between endosomal size and the proton sponge hypothesis. We start from the assumption that a certain amount of polyplex is endocytosed and located inside an endosome of radius $R_0$. Under the proton sponge hypothesis, the buffering action of the polymer will cause an influx of $Cl^-$ ions ($\Delta N$). This in turn causes an influx of $H_2O$ into the endosome, increasing endosomal size to $R$. Hereby, an osmotic pressure ($P_{osm}$) is generated that is described by the "van 't Hoff formula" :

$$P_{osm} = \Delta C k_b T \qquad (1)$$

with $\Delta C = C_e - C_0$ the difference in chloride number concentration in an endosome with ($C_e$) and without ($C_0$) the polymer, $k_b$ the Boltzmann constant and $T$ the absolute temperature. Due to the surface tension $\gamma$ of the endosomal membrane, endosomal swelling will, however, be counteracted by a pressure described by Laplace's law:

$$P_{Lap} = \frac{2\gamma}{R} \qquad (2)$$

When $P_{osm}$ equals $P_{Lap}$, an equilibrium is reached, from which it follows that:

$$\Delta C = \frac{4\kappa\varepsilon d}{k_b T R_0 (1+\varepsilon)} \qquad (3)$$

in which the surface tension was rewritten as $\gamma = 2\kappa\epsilon d$, with $\kappa$ Young's elasticity modulus, $d$ the thickness of the membrane and $\varepsilon = \Delta R / R_0$ the strain.[21] Equation (3) expresses the concentration difference in chloride ions that is needed to let the endosome with initial radius $R_0$ swell to such an extent that the endosomal membrane experiences a strain $\varepsilon$. If we finally rewrite $\Delta C = \Delta N / V_0$, and denoting $\varepsilon_{max}$ as the maximal strain supported by the membrane (*i.e.* the burst criterion), one finally finds:

$$\Delta N = \frac{16\pi\kappa d}{3k_b T} \cdot \frac{\varepsilon_{max}}{1+\varepsilon_{max}} \cdot {R_0}^2 \qquad (4)$$

Equation (4) shows that the number of protons or chloride ions needed to burst an endosome increases with the square of the endosomal radius, *i.e.* proportional to the endosome's surface area. This gives a clear indication as to why endosomal escape in cells with bigger endosomes, as for the ARPE-19 cells, is intrinsically less likely to happen for a given amount of polymer.

*Putting the model to the test*

In order to evaluate the plausibility of Equation (4), several constants used in the formula need to be defined. According to Li *et al.*[22] the elastic limit of phospholipid vesicles is around 5-10% increase in surface area, which can be translated into a burst criterion of 5% endosomal strain ($\varepsilon_{max} = 0.05$; see Supporting

Information 'Defining the burst criterion'). The elastic modulus $\kappa$ of phospholipid vesicles is reported to be in the range of 3 .$10^7$ – 8 .$10^7$ $\frac{N}{m^2}$ [21] and the thickness of the membrane is set to 4.1 nm[23]. The absolute temperature in the cells corresponds to 310 K and $k_b$ equals 1.38 .$10^{-23}$JK$^{-1}$. Based on this information, Equation (4) is plotted in **Figure 6** (dotted line as the upper limit ($\kappa$ = 8 .$10^7$ $\frac{N}{m^2}$) and solid line as the lower limit ($\kappa$ = 3 .$10^7$ $\frac{N}{m^2}$)), showing the quadratic dependence of the endosomal chloride ion influx needed to burst the vesicle as a function of the endosomal radius. Selected values are also presented in Table 1. It is interesting to relate these numbers to the amount of polymer that is actually needed to burst an endosome of a given size. It should be noted that the effective buffering capacity of a JetPEI/pDNA polyplex is only 20% of the free polymer, due to the electrostatic interaction with pDNA and the electrostatic repulsion resulting from protonation of neighboring amine groups.[24] Based on this information, the number of NH-containing monomers that is needed to cause the required $Cl^-$ influx for endosomal bursting can be calculated (**Table 1** and right y-axis of **Fig. 6**).

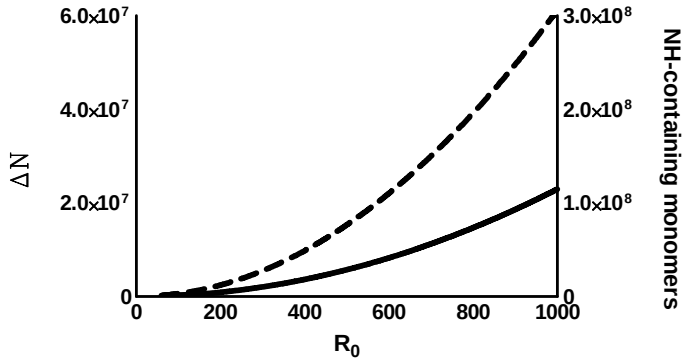


**Fig. 6. Graph to illustrate the influence of endosomal radius ($R_0$) on the amount of chloride ions ($\Delta N$; left y-axis) or NH-containing monomers (right y-axis) needed to induce endosomal bursting (*cfr*. Equation (4) and values mentioned in the main text).** The dotted line represents the upper limit ($\kappa$ = 8 .$10^7$ $\frac{N}{m^2}$) while the solid line indicates the lower limit ($\kappa$ = 3 .$10^7$ $\frac{N}{m^2}$).

As a final step, it is more meaningful to convert these values to the corresponding number of polyplexes. In order to achieve this conversion, we calculated that one polyplex contains on average 1,9 ± 0,2 .$10^6$ NH-containing monomers (calculation in Supporting Information 'Converting NH-containing monomers to the

amount of polyplexes'). Using this average, the number of polyplexes needed to burst an endosome with a given radius was determined and is displayed in **Table 1**.

**Table 1. Overview of the number of chloride ions, NH-containing monomers and corresponding number of JetPEI/pDNA polyplexes needed to burst an endosome of a given radius.** Lower limit is calculated using $\kappa = 3 .10^7 \frac{N}{m^2}$; upper limit is calculated using $\kappa = 8 .10^7 \frac{N}{m^2}$.

| | 200 nm | 400 nm | 600 nm |
|---|---|---|---|
| **Chloride influx ($\Delta N$ in ions)** | $9{,}2.10^5$ - $2{,}5.10^6$ | $3{,}7.10^6$ - $9{,}8.10^6$ | $8{,}3.10^6$ - $2{,}2.10^7$ |
| **NH-containing monomers** | $4{,}6.10^6$ - $1{,}2.10^7$ | $1{,}8.10^7$ - $4{,}9.10^7$ | $4{,}1.10^7$ - $1{,}1.10^8$ |
| **Polyplexes** | 2-7 | 8-28 | 19-62 |

The calculated amount of polyplexes are quite plausible, giving a good indication that Equation (4) provides a reasonable description of swelling and bursting of an endosome by the proton sponge mechanism. Since our results show that HeLa cells have smaller endosomes, they would need to accumulate less polyplexes to efficiently induce endosomal bursting *via* the proton sponge effect. In our opinion, having ruled out many other potential causes, this provides a plausible explanation as to why endosomal escape is more efficient in HeLa cells than in ARPE-19 cells.

***Endosomal leakiness***

While differences in endosomal size can explain the differences in transfection efficiency between HeLa and ARPE-19 cells, it remains quite intriguing why even in the smaller HeLa endosomes, endosomal escape happens in less than 10% of the total amount of polyplex-containing endosomes. This means that an astonishing >90% of the polyplexes do not contribute to the final biological effect. We reasoned that this may perhaps be the result of endosomal membrane leakiness, *i.e.* the loss of its semi-permeable property for small molecules such as chloride ions and water molecules, which would prevent the build-up of osmotic pressure. Such leakiness may in fact be induced by stress on the endosomal membrane due to the gradually increasing osmotic pressure combined with membrane destabilization due to interaction with

the cationic polyplexes. To test this experimentally, calcein was incorporated into endosomes as a model for small molecules. Since it was used in self-quenching concentrations, a subtle leak in the endosomal membrane could be easily witnessed by the change from a punctate fluorescent pattern (endosomes) to a diffuse (dequenched) cytoplasmic fluorescence. The microscopy images in **Figure 7A** confirm that for both HeLa and ARPE-19 cells, calcein is released in virtually every cell that has taken up polyplexes, even in those that do not show release of AF647 labeled ONs. Control cells (incubated with calcein alone) did not show any cytoplasmic fluorescence apart from a punctuate endosomal pattern. Furthermore, a PEI dose curve was performed where cells were incubated with a decreasing concentration of polyplexes in order to evaluate the effect on endosomal leakiness. **Figure 7B** shows the intensity of cytosolic calcein fluorescence after incubation with 1, 1/2, 1/5 and 1/10 dilutions of NPs, clearly indicating that calcein release is dependent on polyplex concentration, thus providing clear evidence that polyplex-containing endosomes do become more leaky to small molecules, which may hinder effective build-up of osmotic pressure and, therefore, endosomal escape.

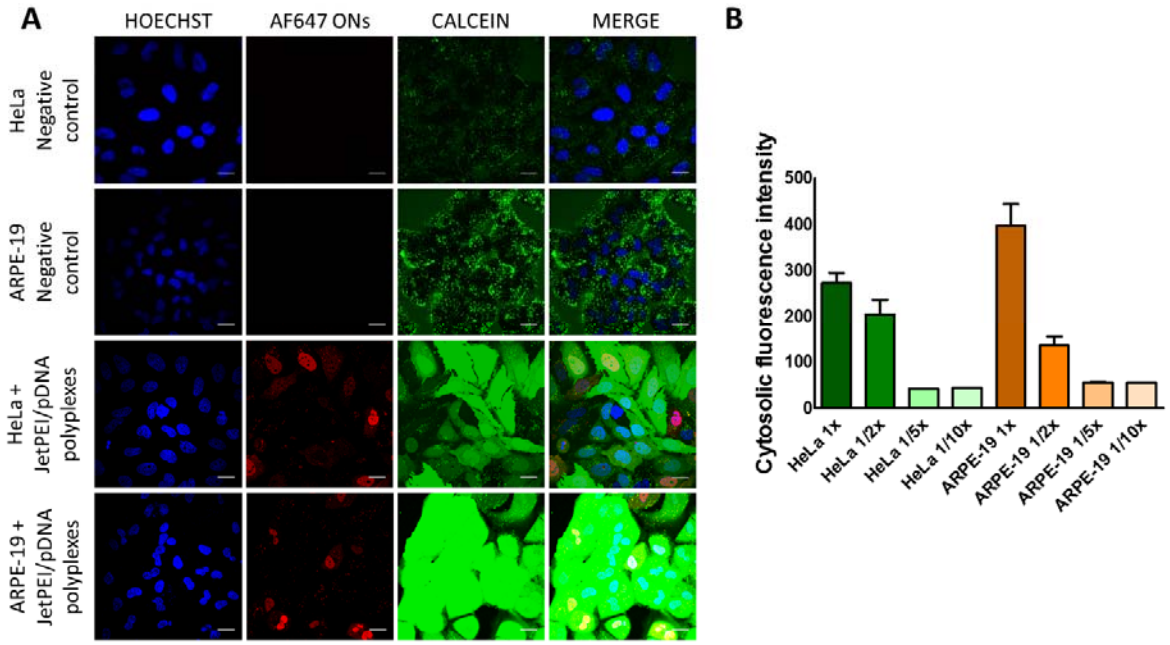


**Fig. 7. Evaluation of endosomal leakiness induced by JetPEI polyplexes. (A)** Hela and ARPE19 cells were incubated with polyplexes and calcein-AM at a self-quenching concentration of 3 mM. The first column shows nuclear staining with Hoechst. The second

column shows AF647 fluorescence, where red nuclei indicate that endosomal escape of AF647 labeled ONs has happened. In the third column, the calcein fluorescence is displayed, where green cells indicate that calcein was able to escape endosomal confinement and leak to the cytoplasm. The last column depicts the merged images. First two rows represent the negative controls (cells incubated with calcein without addition of JetPEI/pDNA polyplexes). The last two rows show images of HeLa and ARPE-19 cells after incubation with both JetPEI polyplexes and calcein. Scale bar represents 25 μm. **(B)** The cytosolic fluorescence intensity of calcein was quantified from microscopy images after incubation with 1x, 1/2x, 1/5x and 1/10x dilutions of the original polyplex concentration, showing that endosomal membrane leakiness is a concentration dependent effect. Graph shows mean ± SEM. In total, 319 HeLa cells and 312 ARPE-19 cells were measured.

### *The interplay between endosomal size and membrane leakiness*

Our results point to endosomal size and membrane leakiness as important factors that determine proton sponge-based endosomal escape in a cell-dependent manner. Hela cells and ARPE19 cells are, however, very different cell types with very different cell division times. Therefore, to further corroborate our findings we included two additional cell lines, A549 and H1299, that match more closely to HeLa cells (A549 22h; H1299 20-23h; HeLa 22h). Both A549 and H1299 cells showed poor transfection efficiency with JetPEI polyplexes, which again could not be attributed to cellular uptake or cytotoxicity (**Fig. 8A-C**; dashed lines indicate results for HeLa cells as a reference). Endosomal escape, however, was again found to be low as measured by ON translocation to the nucleus as before. Only 11.37 ± 0.44 % and 11.12 ± 1.70 % cells showed endosomal escape for A549 and H1299 cells respectively (**Fig. 8D**). Measuring the endosomal size as before, A549 cells have endosomes that are even larger than in ARPE-19 cells, while the endosomes of H1299 cells are even smaller than those of HeLa cells (**Fig. 8E** and **Fig. S3**). Thus, while the presence of large endosomes provides and explanation for the low transfection results in A549 cells, it does not for the H1299 cells.

Next we investigated endosomal leakiness induced by JetPEI polyplexes with the calcein release assay in the four cell types (HeLa, ARPE-19, A549 and H1299) *via* flow cytometry. In order to be able to compare the membrane leakiness between cell lines, calcein fluorescence after addition of polyplexes was corrected for both initial calcein uptake and cell volume. Results are shown in **Figure 8F** and indicate that HeLa, ARPE-19 and A549 have similar, rather low levels of membrane leakiness, indicating that endosomal

leakiness is independent of endosomal size. On the other hand, H1299 endosomes showed markedly more endosomal membrane leakiness, which explains low endosomal escape efficiency in these cells in spite of their smaller endosomes. Based on these results, we can conclude that endosomal escape efficiency by the proton sponge mechanism depends on both endosomal leakiness and endosomal size, which is cell-type dependent. When membrane leakiness is comparable between cell lines (*e.g.* HeLa *vs* ARPE-19 *vs* A549) endosomal escape efficiency is correlated to endosomal size: when endosomal size increases, endosomal escape becomes less feasible. However, when vesicles exhibit extreme leakiness (*e.g.* H1299), even a small endosomal size will not induce high rates of endosomal escape since the vesicles are unable to sufficiently build up osmotic pressure.

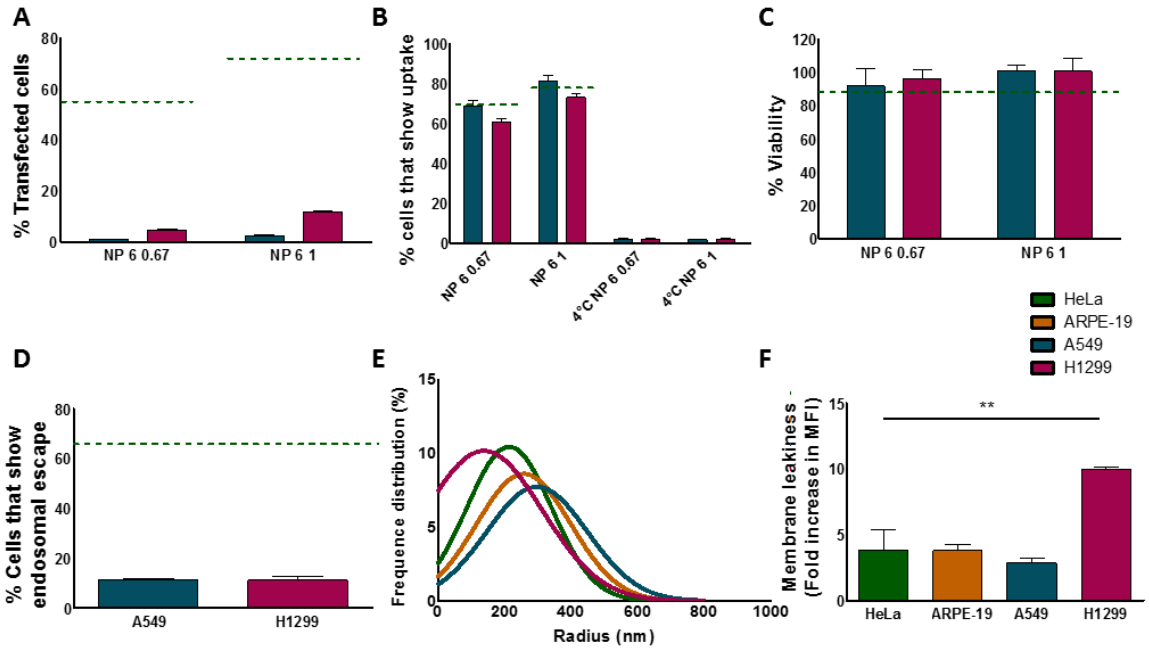


**Fig. 8. Evaluation of A549 and H1299 cells. (A)** Transfection efficiency expressed as percentage of transfected cells. Graph shows mean ± SEM; n=3 **(B)** Polyplex uptake is shown as the percentage of cells that show uptake. Graph shows mean ± SEM; n=2. **(C)** Toxicity was evaluated by means of an MTT test. Graph shows mean ± SEM; n=2. **(D)** Endosomal escape was evaluated 6h after addition of polyplexes (NP 6 0.67µg pDNA) to the cells. Graph represents mean ± SEM after evaluation of 713 A549 cells and 780 H1299 cells. For graphs **A-D** a dotted green line was added to compare the values with the reference value as measured on HeLa cells. **(E)** The size of 1008 A549 and 942 H1299 endosomes was measured after incubation with FITC dextrans and subsequent chase with cell culture medium for 3h. A Gaussian fit was performed on the frequence distributions of endosomal radii from **figure S3** and were compared to the Gaussian fit performed for HeLa and ARPE-19 cells to show the variability in endosomal sizes. **(F)** Membrane leakiness evaluated by measuring calcein fluorescence *via* flow cytometry. Values were corrected for initial calcein uptake and cell volume. The fold increase of calcein fluorescence was calculated after incubation with JetPEI NP 6 0.67 particles for 15min and subsequent chase for 3h *vs* calcein uptake without addition of particles. Graph shows mean ± SEM; n=2.

## DISCUSSION

Endosomal escape has been identified as one of the main bottlenecks in gene delivery[2,4,10–12] and the interest in this barrier has spiked in the last decade. This is reflected by the growing number of publications on this topic, which has increased 10x since 2000.[25] However, trial and error and empirical experimental approaches have predominantly driven the field of nanoparticle design. Recently, critical voices are emerging saying it is time to change course towards a more rational approach of nanoparticle design, taking into consideration the complex series of biological barriers.[26] It is now thought that an enhanced fundamental understanding of cell biology coupled with innovations in material science will be beneficial for the development of a new generation of synthetic carriers.[10,27–29]

In line with this view, we tried to get a better insight into the factors that influence proton sponge-based endosomal escape of polymer gene carriers, which was enabled by recent developments that made detection and visualization of this elusive event possible by high-end live cell microscopy.[2,11,30] Our work was inspired by the observation that polyplexes induced a markedly higher transfection efficiency in HeLa cells as compared to ARPE-19 cells. Cellular experiments revealed that the difference in transfection was not based on a variation in toxicity or an increase in cellular uptake of the polyplexes in HeLa cells. On the contrary: uptake was even found to be higher in ARPE-19 cells than in HeLa cells. Next, using a specific dequenching assay in live-cell spinning disk and swept field confocal microscopy, the endosomal escape capacity of JetPEI/pDNA polyplexes was evaluated directly.[16] With automated image processing, >1000 cells were analyzed, revealing that JetPEI/pDNA polyplexes induce on average about 9 times more endosomal escape events in HeLa cells as in ARPE-19 cells (**Fig. 4D**). This finding is illustrative of the current view that on the intracellular level endosomal escape is indeed one of the most prominent – and perhaps least understood – barriers to effective gene delivery.[4,12,31] Even though there are several barriers that still may play a role after the endosomal barrier (*e.g.* vector unpacking, nuclear uptake), transfection efficiency is clearly linked to the extent to which endosomal escape happens. We reckoned that this marked

difference between both cell types would be an interesting starting point to find out more about the factors that govern proton sponge-based endosomal escape.

***Endosomal sequestration, pH and mobility***

If HeLa cells would internalize and sequester polyplexes to a higher extent than ARPE-19 cells, this could explain the higher endosomal escape frequency since it has been stated before that a critical threshold exists for polymers to mediate endosomal escape through the proton sponge effect.[32,33] However, our results indicated that the number of polyplexes per endosome was actually lower in HeLa cells than in ARPE-19 cells since HeLa cells internalized less polyplexes (**Fig. 2E**) and distributed them over more endosomes (**Fig. 4A**) as illustrated in **Figure 4B**. Furthermore, endosomal escape cannot be considered a game of chances since a doubling in number of endosomes cannot account for the 9 times increase in endosomal escape frequency. Next, since pH is a major determinant of the proton sponge hypothesis, it is obvious that it could have a significant impact on endosomal escape. pH measurements confirmed a rapid (<15 min) drop in intravesicular pH to 6.5, reaching an equilibrium at around pH 5.5 as expected.[34–36] However, the endosomal pH in ARPE-19 endosomes was found to be slightly lower than the pH in HeLa endosomes, so that differences regarding endosomal escape capacities could not be attributed to a difference in intrinsic pH value of the endosomes (**Fig. 5A**). Thereafter it was hypothesized that the mobility of endosomes could have an impact on endosomal escape frequencies in two different manners. First, the shear stress on the vesicle membrane caused by the migration of the endosomes through the cytoplasm could result in a destabilization of the endosomal membrane. Second, greater endosomal mobility could result in higher energy collisions with other cell organelles or the cytoskeleton, which could lead to endosomal bursting. Quantitative analysis of endosomal mobility by single particle tracking microscopy did, however, not reveal clear differences between the two cell types. If anything, ARPE-19 cells showed a slightly increased mobility when compared to HeLa cells (**Fig. 5B**).

***Endosomal size***

When inspecting the confocal microscopy images, a rather marked difference between both cell types was that ARPE-19 cells appeared to have larger endosomes than HeLa cells, which was confirmed by quantifying the endosomal size (**Fig. 5C-D**). We hypothesized that this might be an important parameter for proton sponge-based endosomal escape. In literature, some reports already indicated a possible relation between endosomal size and transfection efficiency. For instance, Lagache *et al.* developed a biophysical model to describe the escape of small nonenveloped viruses from endosomes triggered by low pH-mediated conformational changes of viral endosomolytic proteins. Their model showed that viral escape time should increase with endosomal size and decrease with the number of viral particles inside the endosome.[37] Barua and Rege found that treatment with tubacin, which acetylates tubulin of microtubules in the cytoplasm, abolished polyplex sequestration at the perinuclear recycling compartment/microtubule organizing center, thereby increasing transgene expression up to forty-fold. The authors hypothesized that distribution of polyplexes in smaller vesicles throughout the cytoplasm as opposed to aggregation at a single large perinuclear region, could allow for greater endosomal escape, which in turn could enhance transfection.[38]

To better understand the relation between endosomal size and proton sponge-based endosomal escape, a simple mathematical model was introduced describing endosomal burst by the proton sponge effect, taking into account both osmotic pressure and the counteracting Laplace pressure. By balancing both opposing forces, we found that the endosomal chloride influx ($\Delta N$) needed to induce endosomal rupture is proportional to the square of the (original) endosomal radius (${R_0}^2$). This can be easily appreciated as being the result of the combined influence of the proton sponge effect causing a change in volume (proportional to ${R_0}^3$) and the counteracting influence of Laplace's law (proportional to $\frac{1}{R_0}$). This simple mathematical model gives support to our hypothesis that large endosomes, as in ARPE-19 cells, are more difficult to burst: an endosome of double the size needs 4 times more polymer to burst. However, we

would like to note that some factors were not considered while setting up this model. First there is the contribution by free polymer that is dissolved in the cell medium upon incubation with the polyplexes and that is endocytosed alongside the polyplexes. Indeed, upon preparation of polyplexes, not all polymer will be incorporated into the particles but a fraction remains free in solution.[39] As such there will be free polymer present in the lumen of the endosomes as well. However, this fraction of dissolved PEI polymer gives a negligible contribution to the osmotic pressure, as explained in Supporting Information ("Amount of NH-containing monomers per endosome from free PEI in solution"), and can be safely disregarded. The second factor that we did not consider is the fraction of free PEI polymer that is electrostatically attracted to the negatively charged cell membrane. Upon endocytosis of polyplexes, *i.e.* by invagination of the cell membrane, it seems likely that the inside of the endosomal membrane will be coated with a layer of membrane-attached polymer. While this fraction of membrane-associated polymer may significantly contribute to the osmotic pressure, it does not matter in our discussion on the role of endosomal size. Indeed, being proportional to the endosomal surface area it only gives a constant offset to the prefactor in Equation (4), but does not change the above considerations on larger endosomes requiring more polyplexes to induce endosomal escape. Finally, disassembly of pDNA from the polyplex could also increase the buffer capacity of the polymer as amines that were used to complex pDNA are now available again to buffer protons. However, we do not have indications to believe that polyplex disassembly happens faster or more efficiently in smaller endosomes than bigger ones. Together this does mean that the number of polyplexes in Table 1 needed to cause endosomal bursting can slightly vary according to the amount of polymer that is attracted to the cell membrane and the disassembly of the polyplex in the endosomal lumen.

It should also be noted that endosomal size is only half the argument. Endosomal trafficking is a highly dynamic process where payloads can be transferred or accumulated during trafficking. As such it cannot be excluded that within a cell larger endosomes may burst if they contain a high polyplex content. For

instance, an endosome of twice the size can theoretically contain 8 times as much polymer, which is more than the factor of 4 that is minimally needed to induce endosomal escape. Therefore, one should not expect that endosomal escape only happens in the smallest endosomes within a cell as trafficking plays a role as well. In any case, while the mathematical model presented in this paper is a simplified representation that only describes the equilibrium state, it does capture the essence that differences in endosomal size can play a decisive role in the inherent capacity of polymer carriers to induce endosomal escape and correlates with the fact that less endosomal escape is seen in ARPE-19 cells. Nevertheless, in future work it would be interesting to explore more extensive computational models of the proton sponge effect, such as the one by Freeman *et al*. for dendrimers that can give a detailed time-dependent description of the proton sponge effect.[40]

With the fundamental understanding of the endosomal barrier that follows from our results, it is tempting to contemplate on ways to boost endosomal release and transfection efficiency of non-viral gene therapeutics. Conceptually it would be interesting to find ways to introduce polyplexes in smaller endosomes, as these should rupture more efficiently than larger endosomes. One option could be to target an endosomal pathway where endosomes have a small intrinsic diameter. In this respect, one could consider using a ligand such as folic acid[41] or albumin[42] to target caveolae mediated endocytosis, since it has been reported that this pathway results in the formation of very small endosomes of 60-80 nm in diameter (compared to 120-150 nm after internalization *via* the classical route of clathrin-dependent endocytosis).[5,43] Several reports indeed show an increased transfection efficiency of caveolae-targeted polyplexes compared to unmodified polyplexes.[41,44] Moreover, even though PEI polyplexes are internalized through a combination of caveolae-mediated endocytosis and clathrin mediated endocytosis, it is stated in several papers that only inhibition of caveolae-mediated endocytosis drastically reduces transfection efficiency.[41,45,46] Together it seems that our size argument may explain, at least in part, why caveolin-mediated uptake offers better transfection of PEI polyplexes. Another concept could be to find ways to

sequester more polyplexes in fewer endosomes. Ogris *et al.* found that large aggregates of PEI and pDNA (> 500 nm) were more efficient than small PEI/pDNA polyplexes (80-150 nm), even though the large aggregates were internalized very slowly and to a low extent.[47] Furthermore, controlled aggregation of PEI/pDNA polyplexes at the cell membrane has been shown to induce an increased transfection efficiency *in vivo*, possibly due to elevated levels of cell binding and endosomal release.[48]

A third approach could be to interact with different endosomal proteins such as Rab GTPases, as they are known to be key regulatory factors for endocytosis and are involved in the formation, transport, tethering and fusion of vesicles.[49] Ganley *et al.* described the formation of late endosomes with decreased size and a reduction in the number of multilamellar and dense-tubule-containing late endosomes/lysosomes after siRNA mediated depletion of Rab9.[50] Endosomal morphology can also be influenced by manipulating Rab5 expression since Rab5 regulates membrane docking and fusion events in the early endocytic pathway. Rab5 inhibition is reported to induce a very small endocytic profile, while Rab5 stimulation leads to enlargement of early endosomes and a juxtranuclear localization.[51,52] Furthermore, inhibition or induction of proteins that affect Rab GTPases (*e.g.* Rin1, a Rab5-guanine exchange factor) or other endosomal proteins (*e.g*. SCAMP3, a Secretory Carrier Membrane Protein) have been reported to influence endosomal size.[53,54] Given the complexity of biochemical processes performed in the cell, it is clear that the interaction of all these endosomal proteins makes it difficult to predict the downstream consequences when stimulating or inhibiting one protein. It is may very well be that manipulating protein expression will have many other (unwanted) effects besides reducing endosomal size. Of course, interfering with protein expression is more of theoretical consideration since it requires cell transfections which we are trying to optimize in the first place.

***Endosomal leakiness***

It remains a flagrant observation that even in HeLa cells less than 10% of the polyplex-containing endosomes show escape at some point. We hypothesized that this may be due to leakiness of the

endosomal membrane as the leakage of water and ions from the endosomal lumen to the cytoplasm results in the loss of osmotic pressure and thereby abolishes proton sponge-based endosomal rupture. Endosomal leakiness can be a result of small defects that arise in the endosomal membrane when pressure builds up upon osmotic swelling in combination with interaction of the protonated PEI chains with the endosomal lipid biliayer.[55] Co-incubation of PEI polyplexes with quenched calcein confirmed this hypothesis since both HeLa and ARPE-19 cells that had taken up PEI/pDNA polyplexes showed cytosolic calcein release in virtually every cell whereas calcein remained trapped in endosomes in the absence of polyplexes (**Fig. 7**).

Li *et al.* investigated the elasticity of unilamellar dioleylphosphatidic acid (DOPA) and DOPA-cholesterol (10-25 mol%) vesicles in KCl and sucrose solutions and found that neither the presence nor the concentration of cholesterol had a significant influence on elasticity. They showed that the elastic limit of examined vesicles remained relatively constant with an elastic limit of 3-5% in KCl solutions and 8-10 % in sucrose solutions.[22] Based on these findings, it seems unlikely that membrane composition alone would have a significant effect on endosomal escape frequency. It would therefore be very interesting to study the interaction of protonated PEI chains with different membrane compositions and its effect on membrane leakiness. In this respect, a paper was published very recently by Clark *et al.* who studied the interaction of PEI with endosomal lipids under osmotic stress using synthetic monolayers and vesicles.[56] Moreover, it would be fascinating not only to study the intercellular differences in membrane composition, but also intracellular differences such as different membrane composition resulting from different uptake pathways within the same cell type. This information could lead us towards identifying types of endosomes that are less likely to form these leaks, thereby giving proton sponge-based rupture a better chance at success.

## CONCLUSION

Taken together, our results point to the fact that both endosomal size and polyplex-induced membrane leakiness have a considerable impact on proton sponge-based endosomal escape. Based on rigorous analysis of four different cell types, we conclude that endosomal size largely determines endosomal escape efficiency when cells have comparable polyplex induced membrane leakiness. However, at high levels of membrane leakiness build-up of osmotic pressure is no longer possible, regardless of endosomal size. In future work, it is of interest to further investigate the reasons why endosomal membrane leakiness differs between cell types, and if endosomal escape efficiency can be increased by interfering with endosomal size and endosomal membrane leakiness.

## MATERIALS AND METHODS

### Materials

DMEM/F-12, Opti-MEM, L-Glutamine, Penicillin-Streptomycin solution (5000 IU/ml penicillin and 5000 µg/ml streptomycin) (P/S), Fetal Bovine Serum (FBS), Trypan Blue, 0.25% Trypsin-EDTA and Dulbecco's phosphate-buffered saline 1x without $Ca^{2+}$/$Mg^{2+}$ (DPBS-) were supplied by GibcoBRL (Merelbeke, Belgium). Hoechst 33342, YOYO-1 iodide, 10 kDa FITC dextrans and 10 kDa AF647 dextrans were purchased from Molecular Probes, Erembodegem, Belgium. Other reagents were purchased from Sigma-Aldrich (Bornem, Belgium) unless otherwise specified.

### Cell culture

HeLa cells (cervical adenocarcinoma cells, ATCC CCL-2) were cultured in Dulbecco's modified Eagle's medium supplemented with growth factor F12 (DMEM/F-12) supplemented with 10% FBS, 2 mM L-Glutamine and 100 µg/ml P/S. ARPE-19 cells (retinal pigment epithelial cells, ATCC CRL-2302) were cultured in Dulbecco's modified Eagle's medium supplemented with growth factor F12 (DMEM/F-12) supplemented with 10% FBS, 2 mM L-Glutamine and 50 µg/ml P/S. A549 cells (lung epithelial cells, ATTCC

CCL-185) were cultured in Dulbecco's modified Eagle's medium (DMEM) supplemented with 10% FBS, 2 mM L-Glutamine and 100 µg/ml P/S. H1299 cells (lung epithelial cells derived from metastatic lymph nodes, ATCC-CCL 5803) were cultured in Roswell Park Memorial Institute (RPMI) 1640 medium supplemented with 10% FBS, 2 mM L-Glutamine and 100 µg/ml P/S. Cells were incubated at 37°C in a humidified atmosphere containing 5% $CO_2$. Cellular experiments were performed on cells with a passage number below 25.

**Purification of plasmids**

pGL4.13 and gWIZ GFP (Promega, Leiden, The Netherlands) were amplified in transformed E. Coli bacteria and isolated from this bacteria suspension using a Qiafilter Plasmid Giga Kit (Qiagen, Venlo, The Netherlands). Concentration was determined on a NanoDrop 2000c (Thermo Fisher Scientific, Rockford, IL, USA) by UV absorption at 260 and 280 nm and adjusted to a final concentration of 1 µg/µl with HEPES buffer (20 mM, pH 7.2).

Labeling of pGL4.13 with YOYO-1 iodide (1 mM in DMSO) was performed by adding the dye to the pDNA mixture in a 1:10 ratio. This mixture was incubated in the dark for 4 h before purification by ethanol precipitation. To this end, 0.1 volume of 5 M NaCl and 2.5 volumes of ice-cold ethanol were added to 1 volume of the dye/pDNA suspension. This mixture was incubated at -80°C for 30 min before centrifugation for 30 min at 14000 g. The resulting pellet was washed with RNAse - and DNAse free 70% ethanol and centrifuged again for 10 min. Finally, the pellet was resuspended in fresh HEPES buffer (20 mM, pH 7.2) and the concentration was adjusted to 1 µg/µl after measurement on the NanoDrop 2000c.

**Preparation of polyplexes**

Polyplexes were prepared using commercially available JetPEI (Polyplus transfection, Leusden, The Netherlands). JetPEI/Nucleic Acid (NA) complexes were obtained by mixing the polymer solution with an equal volume of NA solution, which was composed of pDNA (gWIZ GFP or YOYO-1 labeled pGL4.13) and

oligonucleotides (GAA-CTT-CAG-GGT-CAG-CTT-GTT, phosphorothioate linked, concentration 0.1 nmol/µg pDNA; AlexaFluor647 labeled (AF647 ONs) or unlabeled) (Eurogentec, Seraing, Belgium). N/P ratio of the polyplexes was calculated using the formula provided by the manufacturer (Equation 5). Next, the mixture was vortexed for 10 s at 2200 rpm and polyplexes were allowed to stabilize for 15 min before final dilution with HEPES buffer (20 mM, pH 7.2).

$$N/P\ ratio = \frac{7.5\ \ x\ \mu l\ of\ JetPEI}{3\ x\ \mu g\ of\ DNA} \qquad (5)$$

**Characterization of polyplexes**

To evaluate complexation of NAs to the polymer, JetPEI polyplexes (N/P ratio 1-8) were tested with gel electrophoresis. A 1% agarose gel was prepared by dissolving 1 g of agarose (UltraPure Agarose, Invitrogen, Erembodegem, Belgium) in 100 ml of 1 x Tris/Borate/EDTA (TBE) buffer after which GelRed (Biotium, Hayward, CA) was added for detection of NAs. 5 µl of Gel Loading Buffer (Ambion, Merelbeke, Belgium) was added per sample and a total volume of 25 µl was pipetted per lane. As a control, a 1 kb ladder (Bioron GmbH, Ludwigshafen, Germany), uncomplexed pDNA and uncomplexed AF647 ONs were taken along in the run. Gel electrophoresis was performed for 30 min at 100 V and a Kodak digital science camera (Kodak EDAS 120, Rochester, NY) was used to acquire an image of the gel under UV light (Bio-Rad UV transilluminator 2000, California, USA).

For Dynamic Light Scattering measurements, JetPEI polyplexes were prepared as described above and were transferred to disposable folded capillary cells (Malvern, Worcestershire, UK) to determine hydrodynamic diameter, polydispersity index and zeta potential *via* the NanoZS Zetasizer (Malvern Instruments, Hoeilaart, Belgium).

**Evaluation of transfection and uptake efficiency *via* flow cytometry**

Cells were seeded in 24 well plates at 50 000 cells per well and allowed to attach overnight. The next day, polyplexes containing gWIZ GFP and AF647 ONs (for transfection experiments) or YOYO-1 labeled pGL4.13

and unlabeled ONs (for uptake experiments) were prepared as described above. Cells were incubated with polyplexes in Opti-MEM for 15 min at 37°C after which they were washed and cultured for another 24 h (transfection) or 3 h (uptake). Particles, with N/P ratio 6, were applied in concentrations equal to 0.67 µg pDNA (NP 6 0.67) or 1.00 µg pDNA (NP 6 1) per 50 000 cells. For uptake studies, a negative control plate at 4°C was implemented and for all samples external YOYO-1 fluorescence was quenched by applying an ice-cold solution of Trypan Blue (½ diluted in DPBS-) after which the samples were prepared for flow cytometry analysis. For transfection studies, a negative control (using complexes prepared with Lipofectamine 2000 (Invitrogen, CA, USA) and pGL4.13) and a positive control (Lipofectamine and gWIZ GFP) were implemented.

To perform analysis by flow cytometry, cells were detached from the well plates using trypsin and transferred to flow cytometry tubes (BD Falcon, Radnor, USA). Next, cell suspensions were centrifuged at 300 g for 5 min (Bio-Rad DiaCent-12, DieMed GmbH, Cressier, Switzerland) and resuspended in flow buffer (DPBS- / 0.1 % Sodium Azide / 1% Bovine Serum Albumine). Finally, samples were vortexed at 2200 rpm for 10 s (YellowLine TTS2, IKA works, Wilmington, USA) and kept on ice. Flow cytometry was performed (FACS Calibur, BD Biosciences, Erembodegem, Belgium) and green fluorescence was measured on 10 000 events per sample (488 nm excitation with Argon laser and detection with a 530/30 nm bandpass filter). FlowJo software (Treestar Inc, Ashland, USA) was used for analysis.

**Cytotoxicity studies**

Cells were seeded in 24 well plates at 50 000 cells per well and were allowed to attach overnight. The next day, polyplexes were prepared containing gWIZ GFP and AF647 ONs and cells were incubated with polyplexes for 15 min at 37°C in Opti-MEM. Next, cells were washed and incubated for an additional 3 h before addition of 3-(4,5-dimethyl-2-thiazolyl)-2,5-diphenyl-2H-tetrazolium bromide (MTT) solution (1 mg/ml in DPBS). After 3 h, the solution was removed and the newly formed purple formazan crystals were dissolved by addition of DMSO. The plates were covered in aluminum foil and placed on an orbital shaker

(Rotamax 120, Heidolph, Germany) for 45 min at 1200 rpm. As a negative control, blank cells were fixed with a 4 % paraformaldehyde solution to stop metabolic activity. UV absorbance was measured on a plate reader (Wallac Envision, Finland) at 590 nm (metabolic activity) and 690 nm (reference wavelength).

**Visualization and quantification of endosomal escape**

Visualization and quantification of endosomal escape was performed based on a dequenching assay first published by Rehman *et al*.[16] To this end, red-labeled fluorescent oligonucleotides (AF647 ONs; 0,1 nmol per µg pDNA) were co-incorporated into the polyplexes. Upon endosomal escape, the labeled ONs will spread towards the cytoplasm, dequench (indicated by an intense burst of light) and finally accumulate into the nucleus. Cells were seeded in 35 mm CELLview microscopy dishes with glass bottom (Greiner Bio-One, Vilvoorde, Belgium) at a density of 150 000 cells in 1.5 ml. On day 3, cell nuclei were stained with Hoechst 33342 staining (1 mg/ml in $H_2O$; 1000x diluted). Next, polyplexes containing gWIZ GFP and AF647 ONs were added to the cells in Opti-MEM and incubated for 15 min at 37°C. After washing the particles off, the cells were provided with full cell culture medium and were inserted into a stage top incubator (Tokai hit, Shizuoka-ken, Japan) to enable live-cell imaging at optimal environmental conditions (5% $CO_2$, 100% humidity and 37°C). Live-cell imaging was performed using a swept-field confocal (SFC) microscope (Nikon eclipse Ti, Japan) equipped with an MLC 400 B laser box (Agilent technologies, California, USA), SFC scan controller (Prairie Technologies, Middleton, USA), an iXon ultra EMCCD camera (Andor Technology, Belfast, UK) and NIS Elements software (Nikon, Japan). A Plan Apo VC 60x 1.4 NA oil immersion objective lens (Nikon, Japan), equipped with a lens heater (6 Watt temperature controller, Bioptechs, Butler, PA, USA), combined with an additional 1.7x magnification on the camera rendered a pixel size of 160 nm. A large image (8x8 frames) was taken every 30 s for a total period of 6 h using the perfect focus system to secure a good focus on the cells during the time of acquisition. Exposure time was set to 20 msec and a slit width of 35 µm was selected. Movies were analyzed using ImageJ (FIJI) software.

**Determination of pH, mobility, size, leakiness and number of endosomes**

***Cell seeding***

*To evaluate the pH inside the endosomes:* Cells were seeded in glass bottom 96 well plates (Greiner Bio-One, Frickenhausen, Germany) with a density of 10 000 cells in a total volume of 100 µl. On the day of imaging, cell nuclei were stained with Hoechst 33342 staining.

*For evaluating the number of polyplex-containing endosomes, endosomal mobility, endosomal size and endosomal leakiness:* Cells were seeded in 35mm CELLview microscopy dishes with glass bottom with a density of 150 000 cells in 1.5 ml. On the day of imaging, cell nuclei were stained with Hoechst 33342 staining.

***Image acquisition and processing***

*Counting the number of polyplex-containing endosomes:* To visualize cell boundaries, cells were incubated with 5 µM calceinAM in Opti-MEM for 30 min at 37 °C before adding JetPEI polyplexes (containing AF647 ONs). After a 15 min incubation, polyplexes were removed by washing and cell culture medium was added. After 3 h, cells were imaged in the focal plane 2 µm above the coverslip using a Nikon C1si confocal laser scanning microscope system equipped with a Plan Apo VC 60x 1.4 NA oil immersion objective lens (Nikon) and a pixel size of 160nm. Image processing was carried out using custom developed software (IPS in Matlab; details in **Table S1**) to determine the amount of polyplex-containing endosomes within the cell boundaries (**Fig. S4**).

*Measuring endosomal pH:* Cells were incubated at 37°C for 45 min with 100 µl of a mixture of 2 mg/ml 10 kDa FITC dextrans and 1 mg/ml 10 kDa AF647 dextrans in DPBS-. The ratio of fluorescence intensity in the green channel to fluorescence intensity in the red channel ($I_{FITC}/I_{AF647}$) was determined as an indication of endosomal pH since $I_{FITC}$ is dependent of pH and $I_{AF647}$ is independent of pH.[57] After a washing step, the 96 well plate was placed on a spinning disk confocal (SDC) microscope (SFC scan controller, previously

described in the swept field microscope set-up was replaced by a Yokogawa CSU-X confocal spinning disk device (Andor, Belfast, UK)) equipped with a Plan Apo VC 60x 1.4 NA oil immersion objective lens (Nikon, Japan) and an additional 1.5x magnification on the microscope to yield a pixel size of 156 nm. Exposure time was set to 20 msec and images were taken at several time points (5 min, 30 min, 1 h, 2 h, 3 h and 24 h) after the washing step. Endosomal contour determination was performed in Matlab (IPS; details in Table S1). FITC dextrans and AF647 dextrans were considered colocalized if their centers were separated less than the maximum of the respective mean radiuses. When colocalization on the endosome scale was observed, $I_{FITC}/I_{AF647}$ ratio was determined. In order to link experimental ratio values to pH values, a calibration was performed next. Various buffers were prepared (pH 4.5 and 5.0 were citrate buffers, pH 5.5, 6.0, 6.5, 7.0 and 7.5 were 20 mM HEPES buffers) and mixed with FITC dextrans and AF647 dextrans. Calibration ratios were measured, a calibration curve was fitted in Matlab (**Fig. S5**) and with the use of this calibration curve, the experimental $I_{FITC}/ I_{AF647}$ ratios were transformed into pH values.

*Measuring endosomal mobility:* JetPEI polyplexes were added to the cells and incubated at 37°C for 15 min. After washing the cells with Opti-MEM, the dish was placed inside the stage top incubator. Movies of 60 s with a frame rate of 5 frames per second were recorded using the SFC microscope (35 µm slit, exposure time 40 msec) with a pixel size of 107 nm. Videos were recorded on several time points after addition of the particles (30 min, 1 h, 2 h and 3 h). Matlab software (IPS; details in **Table S1**) was used to determine the contours of the endosomes and motion trajectories of individual endosomes were obtained *via* Matlab software (Supporting Information 'Image processing – mobility analysis in Matlab') and were used to calculate endosomal velocity.

*Determination of endosomal size:* After incubation with 2 mg/ml 10 kDa FITC dextrans for 45 min in 37°C, cells were washed and chased with cell culture medium for 3 h. Imaging was performed using the SDC with a pixel size of 92 nm. Next, contours of the FITC-containing endosomes were determined (IPS; details in **Table S1**) and a distribution of endosomal radiuses was generated.

*Evaluation of endosomal leakiness:* Cells were incubated with JetPEI polyplexes for 15 min at 37 °C. After washing off the polyplexes, endosomes were stained with calcein in self quenching concentration (3 mM) for 15 min. Cells were washed with Opti-MEM and incubated for another 3 h before confocal images were acquired using a Nikon C1si confocal laser scanning microscope system equipped with a Plan Apo VC 60x 1.4 NA oil immersion objective lens (Nikon) and a pixel size of 210 nm. Afterwards, cells were trypsinized and their diameter was measured, again *via* confocal microscopy. Finally, samples were prepared for analysis *via* flow cytometry.

**Determining the amount of NH-containing monomers per JetPEI/pDNA polyplex**

In order to determine the number of NH-containing monomers per JetPEI/pDNA polyplex, polyplexes with N/P 6, were prepared as described previously, containing gWIZ GFP and AF647 ONs, and diluted to 50 ml with HEPES (20 mM, pH 7.2). Next, polyplex concentration was measured *via* nanoparticle tracking analysis using the NanoSight LM10 (Malvern, Worcestershire, UK). Measurements were recorded in quintuplet. Based on the theoretical number of pDNA and ON strands added during preparation of the polyplexes and the obtained polyplex concentration, it was possible to determine the average number of pDNA and ON strands per polyplex and thereby calculate the amount of NH-containing monomers per JetPEI/pDNA polyplex.

**Statistical analysis**

All statistical analysis were performed using GraphPad software (La Jolla, CA, USA) and propagation of errors was applied when necessary. Number of asterisks in figures indicates statistical significance: *** $p < 0.0001$; ** $p < 0.01$; * $p < 0.05$.

## ACKNOWLEDGEMENTS

L. Vermeulen would like to acknowledge the financial support of the Agency for Innovation by Science and Technology in Belgium. Financial support by the Ghent University Special Research Fund and the Fund for Scientific Research Flanders (FWO, Belgium) is acknowledged with gratitude. This research was funded by the European Research Council (ERC) under the European Union's Horizon 2020 research and innovation program (grant agreement [648214]) and has received support from the Innovative Medicines Initiative Joint Undertaking under grant agreement n° 115363 resources of which are composed of financial contribution from the European Union's Seventh Framework Programme (FP7/2007-2013) and EFPIA companies' in kind contribution.

## SUPPORTING INFORMATION

One supporting Information document is available that consists of 5 additional figures, 1 additional table, the derivation to define the burst criterion, the conversion of NH-containing monomers to the amount of polyplexes, the amount of NH-containing monomers per endosome due to free PEI in solution and information regarding image processing. Five supporting movies are also available. This material is available free of charge *via* the Internet at http://pubs.acs.org.

## REFERENCES

(1) Jhaveri, A.; Torchilin, V. Intracellular Delivery of Nanocarriers and Targeting to Subcellular Organelles. *Expert Opin. Drug Deliv.* **2016**, *13*, 49–70.

(2) Lönn, P.; Kacsinta, A. D.; Cui, X.-S.; Hamil, A. S.; Kaulich, M.; Gogoi, K.; Dowdy, S. F. Enhancing Endosomal Escape for Intracellular Delivery of Macromolecular Biologic Therapeutics. *Sci. Rep.* **2016**, *6*, 1-9.

(3) Rajendran, L.; Knölker, H.-J.; Simons, K. Subcellular Targeting Strategies for Drug Design and Delivery. *Nat. Rev. Drug Discov.* **2010**, *9*, 29–42.

(4) Martens, T. F.; Remaut, K.; Demeester, J.; De Smedt, S. C.; Braeckmans, K. Intracellular Delivery of Nanomaterials: How to Catch Endosomal Escape in the Act. *Nano Today* **2014**, *9*, 344–364.

(5) Sahay, G.; Alakhova, D. Y.; Kabanov, A. V. Endocytosis of Nanomedicines. *J. Control. Release* **2010**, *145*, 182–195.

(6) Canton, I.; Battaglia, G. Endocytosis at the Nanoscale. *Chem. Soc. Rev.* **2012**, *41*, 2718–2739.

(7) Iversen, T. G.; Skotland, T.; Sandvig, K. Endocytosis and Intracellular Transport of Nanoparticles: Present Knowledge and Need for Future Studies. *Nano Today* **2011**, *6*, 176–185.

(8) Akinc, A.; Battaglia, G. Exploiting Endocytosis for Nanomedicines. *Cold Spring Harb. Perspect. Biol.* **2013**, *5*, 1-24.

(9) Pangarkar, C.; Dinh, A. T.; Mitragotri, S. Endocytic Pathway Rapidly Delivers Internalized Molecules to Lysosomes: An Analysis of Vesicle Trafficking, Clustering and Mass Transfer. *J. Control. Release* **2012**, *162*, 76–83.

(10) Stewart, M. P.; Lorenz, A.; Dahlman, J.; Sahay, G. Challenges in Carrier-Mediated Intracellular Delivery: Moving beyond Endosomal Barriers. *Wiley Interdiscip. Rev. Nanomedicine Nanobiotechnology* **2016**, *8*, 465–478.

(11) Gilleron, J.; Querbes, W.; Zeigerer, A.; Borodovsky, A.; Marsico, G.; Schubert, U.; Manygoats, K.; Seifert, S.; Andree, C.; Stöter, M.; Epstein-Barash, H.; Zhang, L.; Koteliansky, V.; Fitzgerald, K.; Fava, E.; Bickle, M.; Kalaidzidis, Y.; Akinc, A.; Maier, M.; Zerial, M. Image-Based Analysis of Lipid Nanoparticle–mediated siRNA Delivery, Intracellular Trafficking and Endosomal Escape. *Nat. Biotechnol.* **2013**, *31*, 638–646.

(12) Shete, H. K.; Prabhu, R. H.; Patravale, V. B. Endosomal Escape: A Bottleneck in Intracellular Delivery. *J. Nanosci. Nanotechnol.* **2014**, *14*, 460–474.

(13) Remaut, K.; Sanders, N. N.; De Geest, B. G.; Braeckmans, K.; Demeester, J.; De Smedt, S. C. Nucleic Acid Delivery: Where Material Sciences and Bio-Sciences Meet. *Mater. Sci. Eng. R Reports* **2007**, *58*, 117–161.

(14) Pack, D. W.; Hoffman, A. S.; Pun, S.; Stayton, P. S. Design and Development of Polymers for Gene Delivery. *Nat. Rev. Drug Discov.* **2005**, *4*, 581–593.

(15) Behr, J. The Proton Sponge: A Trick to Enter Cells the Viruses Did Not Exploit. *Int. J. Chem.* **1997**, *2*, 34–36.

(16) Rehman, Z. U.; Hoekstra, D.; Zuhorn, I. S. Mechanism of Polyplex- and Lipoplex-Mediated Delivery of Nucleic Acids: Real-Time Visualization of Transient Membrane Destabilization without Endosomal Lysis. *ACS Nano* **2013**, *7*, 3767–3777.

(17) Lv, H.; Zhang, S.; Wang, B.; Cui, S.; Yan, J. Toxicity of Cationic Lipids and Cationic Polymers in Gene Delivery. *J. Control. Release* **2006**, *114*, 100–109.

(18) Wang, C.; de Jong, E.; Sjollema, K. A.; Zuhorn, I. S. Entry of PIP3-Containing Polyplexes into MDCK Epithelial Cells by Local Apical-Basal Polarity Reversal. *Sci. Rep.* **2016**, *6*, 1-13.

(19) Weng, T.; Rein, D. H.; Dean, B.J.; Stabila, P. F.; Goddard, M. B. I. Arpe-19 as a Platform Cell Line for Encapsulated Cell-Based Delivery. *United States Patent (US 6,361,771 B1)* **2002**.

(20) Posakony, J. W.; England, J. M.; Attardi, G. Mitochondrial Growth and Division During the Cell Cycle in Hela Cells. *J. Cell Biol.* **1977**, *74*, 468–491.

(21) Hallett, F. R.; Marsh, J.; Nickel, B. G.; Wood, J. M. Mechanical Properties of Vesicles. A Model for Osmotic Swelling and Lysis. *Biophys. J.* **1993**, *64*, 435–442.

(22) Li, W.; Aurora, T. S.; Haines, T. H.; Cummins, H. Z. Elasticity of Synthetic Phospholipid Vesicles and Submitochondrial Particles during Osmotic Swelling. *Biochemistry* **1986**, *25*, 8220–8229.

(23) Rutkowski, C. a; Williams, L. M.; Haines, T. H.; Cummins, H. Z. The Elasticity of Synthetic Phospholipid Vesicles Obtained by Photon Correlation Spectroscopy. *Biochemistry* **1991**, *30*, 5688–5696.

(24) Ziebarth, J. D.; Wang, Y. Understanding the Protonation Behavior of Linear Polyethylenimine in Solutions through Monte Carlo Simulations. *Biomacromolecules* **2011**, *11*, 1–29.

(25) Medline (PubMed) Trend http://dan.corlan.net/medline-trend.html (accessed Jan 4, 2017).

(26) Blanco, E.; Shen, H.; Ferrari, M. Principles of Nanoparticle Design for Overcoming Biological Barriers to Drug Delivery. *Nat. Biotechnol.* **2015**, *33*, 941–951.

(27) Yin, H.; Kanasty, R. L.; Eltoukhy, A. A.; Vegas, A. J.; Dorkin, J. R.; Anderson, D. G. Non-Viral Vectors for Gene-Based Therapy. *Nat. Rev. Genet.* **2014**, *15*, 541–555.

(28) Bishop, C. J.; Kozielski, K. L.; Green, J. J. Exploring the Role of Polymer Structure on Intracellular Nucleic Acid Delivery *via* Polymeric Nanoparticles. *J. Control. Release* **2015**, *219*, 488–499.

(29) Editorial. Time to Deliver. *Nat. Biotechnol.* **2014**, *32*, 961.

(30) Wittrup, A.; Ai, A.; Liu, X.; Hamar, P.; Trifonova, R.; Charisse, K.; Manoharan, M.; Kirchhausen, T.; Lieberman, J. Visualizing Lipid-Formulated siRNA Release from Endosomes and Target Gene Knockdown. *Nat. Biotechnol.* **2015**, *33*, 870–876.

(31) Varkouhi, A. K.; Scholte, M.; Storm, G.; Haisma, H. J. Endosomal Escape Pathways for Delivery of Biologicals. *J. Control. Release* **2011**, *151*, 220–228.

(32) Kichler, A.; Leborgne, C.; Coeytaux, E.; Danos, O. Polyethylenimine-Mediated Gene Delivery: A Mechanistic Study. *J. Gene Med.* **2001**, *3*, 135–144.

(33) Richard, I.; Thibault, M.; De Crescenzo, G.; Buschmann, M. D.; Lavertu, M. Ionization Behavior of Chitosan and Chitosan-DNA Polyplexes Indicate That Chitosan Has a Similar Capability to Induce a Proton-Sponge Effect as PEI. *Biomacromolecules* **2013**, *14*, 1732–1740.

(34) Geisow, J.; Evans, W. H. pH in the Endosome - Measurement during Pinocytosis and Receptor-Mediated Endocytosis. *Cell* **1984**, *150*, 36–46.

(35) Huotari, J.; Helenius, A. Endosome Maturation. *EMBO J.* **2011**, *30*, 3481–3500.

(36) Wang, C.; Zhao, T.; Li, Y.; Huang, G.; White, M. A.; Gao, J. Investigation of Endosome and Lysosome Biology by Ultra pH-Sensitive Nanoprobes. *Adv. Drug Deliv. Rev.* **2016**, *113*, 87-96.

(37) Lagache, T.; Danos, O.; Holcman, D. Modeling the Step of Endosomal Escape during Cell Infection by a Nonenveloped Virus. *Biophys. J.* **2012**, *102*, 980–989.

(38) Barua, S.; Rege, K. The Influence of Mediators of Intracellular Trafficking on Transgene Expression Efficacy of Polymer-Plasmid DNA Complexes. *Biomaterials* **2010**, *31*, 5894–5902.

(39) Benjaminsen, R. V; Mattebjerg, M. A.; Henriksen, J. R.; Moghimi, S. M.; Andresen, T. L. The Possible "Proton Sponge " Effect of Polyethylenimine (PEI) Does Not Include Change in Lysosomal pH. *Mol. Ther.* **2013**, *21*, 149–157.

(40) Freeman, E. C.; Weiland, L. M.; Meng, W. S. Modeling the Proton Sponge Hypothesis: Examining Proton Sponge Effectiveness for Enhancing Intracellular Gene Delivery through Multiscale Modeling. *J. Biomater. Sci. Polym. Ed.* **2013**, *24*, 398–416.

(41) Gabrielson, N. P.; Pack, D. W. Efficient Polyethylenimine-Mediated Gene Delivery Proceeds *via* a Caveolar Pathway in HeLa Cells. *J. Control. Release* **2009**, *136*, 54–61.

(42) Wang, Z.; Tiruppathi, C.; Minshall, R. D.; Malik, A. B. Size and Dynamics of Caveolae Studied Using Nanoparticles in Living Endothelial Cells. *ACS Nano* **2009**, *3*, 4110–4116.

(43) El-Sayed, A.; Harashima, H. Endocytosis of Gene Delivery Vectors: From Clathrin-Dependent to Lipid Raft-Mediated Endocytosis. *Mol. Ther.* **2013**, *21*, 1118–1130.

(44) Cao, D.; Tian, S.; Huang, H.; Chen, J.; Pan, S. Divalent Folate Modification on PEG: An Effective Strategy for Improving the Cellular Uptake and Targetability of PEGylated Polyamidoamine − Polyethylenimine Copolymer. *Mol. Pharm.* **2015**, *12*, 240–252.

(45) Rejman, J.; Bragonzi, A.; Conese, M. Role of Clathrin- and Caveolae-Mediated Endocytosis in Gene Transfer Mediated by Lipo- and Polyplexes. *Mol. Ther.* **2005**, *12*, 468–474.

(46) Van Der Aa, M. A. E. M.; Huth, U. S.; Häfele, S. Y.; Schubert, R.; Oosting, R. S.; Mastrobattista, E.; Hennink, W. E.; Peschka-Süss, R.; Koning, G. A.; Crommelin, D. J. A. Cellular Uptake of Cationic Polymer-DNA Complexes *via* Caveolae Plays a Pivotal Role in Gene Transfection in COS-7 Cells. *Pharm. Res.* **2007**, *24*, 1590–1598.

(47) Ogris, M.; Steinlein, P.; Carotta, S.; Brunner, S.; Wagner, E. DNA/polyethylenimine Transfection Particles: Influence of Ligands, Polymer Size, and PEGylation on Internalization and Gene Expression. *AAPS PharmSci* **2001**, *3*, 43–53.

(48) Wightman, L.; Kircheis, R.; Rössler, V.; Garotta, S.; Ruzicka, R.; Kursa, M.; Wagner, E. Different Behavior of Branched and Linear Polyethylenimine for Gene Delivery *in Vitro* and *in Vivo*. *J. Gene Med.* **2001**, *3*, 362–372.

(49) Hutagalung, A. H.; Novick, P. J. Role of Rab GTPases in Membrane Traffic and Cell Physiology. *Physiol. Rev.* **2011**, *91*, 119–149.

(50) Ganley, I. G.; Carroll, K.; Bittova, L.; Pfeffer, S. Rab9 GTPase Regulates Late Endosome Size and Requires Effector Interaction for Its Stability. *Mol. Biol. Cell* **2004**, *15*, 5420–5430.

(51) Nielsen, E.; Severin, F.; Backer, J. M.; Hyman, A. A.; Zerial, M. Rab5 Regulates Motility of Early Endosomes on Microtubules. *Nat. Cell Biol.* **1999**, *1*, 376–382.

(52) Stenmark, H.; Parton, R. G.; Steele-Mortimer, O.; Lütcke, A.; Gruenberg, J.; Zerial, M. Inhibition of rab5 GTPase Activity Stimulates Membrane Fusion in Endocytosis. *EMBO J.* **1994**, *13*, 1287–1296.

(53) Galvis, A.; Giambini, H.; Villasana, Z.; Barbieri, M. A. Functional Determinants of Ras Interference 1 Mutants Required for Their Inhbitory Activity on Endocytosis. *Exp. Cell Res.* **2009**, *315*, 820–835.

(54) Thomas, P.; Wohlford, D.; Aoh, Q. L. SCAMP-3 Is a Novel Regulator of Endosomal Morphology and Composition. *Biochem. Biophys. Res. Commun.* **2016**, *478*, 1028-1034.

(55) Choudhury, C. K.; Kumar, A.; Roy, S. Characterization of Conformation and Interaction of Gene Delivery Vector Polyethylenimine with Phospholipid Bilayer at Different Protonation State. *Biomacromolecules* **2013**, *14*, 3759–3768.

(56) Clark, S. R.; Lee, K. Y.; Lee, H.; Khetan, J.; Kim, H. C.; Choi, Y. H.; Shin, K.; Won, Y.-Y. Determining the Effects of PEI Adsorption on the Permeability of DPPC/BMP Membranes under Osmotic Stress. *Acta Biomater.* **2017**, *65*, 317-326.

(57) Geisow, M. J. Fluorescein Conjugates as Indicators of Subcellular pH. A Critical Evaluation. *Exp. Cell Res.* **1984**, *150*, 29–35.